Front. Struct. Civ. Eng. 2022, 16(10): 1301–1314
https://doi.org/10.1007/s11709-022-0883-4

RESEARCH ARTICLE

Experimental study and assessment of thermal energy storage mortar with paraffin/recycled brick powder composite phase change materials

Luchen HAO[a], Jianzhuang XIAO[a*], Wanzhi CAO[b], Jingting SUN[c]

[a] *Department of Structural Engineering, Tongji University, Shanghai 200092, China*
[b] *College of Civil Engineering, Northwest Minzu University, Lanzhou 730024, China*
[c] *Postdoctoral Station of Mechanical Engineering, Tongji University, Shanghai 200092, China*
[*] *Corresponding author. E-mail: jzx@tongji.edu.cn*

ABSTRACT Thermal energy storage recycled powder mortar (TESRM) was developed in this study by incorporating paraffin/recycled brick powder (paraffin/BP) composite phase change materials (PCM). Fourier transform infrared and thermogravimetric analysis results showed that paraffin/BP composite PCM had good chemical and thermal stability. The onset melting temperature and latent heat of the composite PCM were 46.49 °C and 30.1 $J \cdot g^{-1}$. The fresh mortar properties and hardened properties were also investigated in this study. Paraffin/BP composite PCM with replacement ratio of 0%, 10%, 20%, and 30% by weight of cement were studied. The results showed that the static and dynamic yield stresses of TESRM were 699.4% and 172.9% higher than those of normal mortar, respectively. The addition of paraffin/BP composite PCM had a positive impact on the mechanical properties of mortar at later ages, and could also reduce the dry shrinkage of mortar. The dry shrinkage of TESRM had a maximum reduction about 26.15% at 120 d. The thermal properties of TESRM were better than those of normal mortar. The thermal conductivity of TESRM was 36.3% less than that of normal mortar and the heating test results showed that TESRM had good thermal energy storage performance.

KEYWORDS recycled powder mortar, recycled brick powder, thermal energy storage, paraffin, phase change material

1 Introduction

The construction industry consumes about 30% of global energy and emits large amounts of carbon dioxide all over the world. In recent years, building energy consumption and emissions of greenhouse gases by the construction industry have increased at annual rates of 2.5% and 1%, respectively [1,2]. Energy efficiency of construction activity has drawn more and more attention and is now an important research topic worldwide. Heat energy reserve technologies can facilitate energy saving within buildings, thus greatly improving the energy efficiency of buildings. As phase change materials (PCM) has a remarkable energy reserve capacity and a narrow temperature window of operation, the incorporation of PCM and heat energy reserve materials has become one popular strategy for improving building energy efficiency [3]. Among the various organic PCMs used in the building sector, paraffin is one of the most popular due to its distinctive specific latent heat, good consistency chemically and non-phase segregation during the melting-freezing process [4–6]. However, because of the representative solid-to-liquid phase transition features, the application of PCM in building requires a form-stable composite that can use a variety of porous materials as matrices to provide support [7]. Various materials have been used to support paraffin composite PCM, such as expanded graphite [8], carbon form [9], diatomite [10], expanded vermiculite [6], expanded perlite [11], recycled brick/block aggregates (RBA) [12,13], etc.

Phase change materials have remarkable thermal energy storage capacity. To improve thermal performance

Article history: Received Sep 22, 2021; Accepted Jul 13, 2022

and building energy efficiency, thermal energy storage materials by incorporating PCM into some construction materials have been developed. Wang et al. [14] prepared two types of heat energy storage concrete by using fatty acids to incorporate diatomite in one type and ceramist in the other. These kinds of thermal energy storage concrete can significantly reduce the room temperature and heat transfer coefficient in summer conduction. Consequently, the use of air conditioning systems and associated energy consumption are reduced. Some researchers also studied the effects of microencapsulation PCM on concrete properties [7,15,16]. Due to its high heat storage rate per volume unit, the microencapsulation PCM has a great positive effect on the thermal properties of concrete. However, despite the fact that these commercial microencapsulated PCMs show positive thermal effects on the developed heat energy storage concrete, they also have many disadvantages, especially incompatibility with concrete matrices. Various studies have found that microcapsules break during the mixing or loading of concrete with microencapsulation PCM [17–19]. Hunger et al. [7] reported that the microencapsulated PCMs shells were broken due to collision and abrasion with aggregate during concrete mixing. Jayalath et al. [18] found that the damage to microencapsulated PCM during the loading stage of hardened concrete was higher than that during the mixing stage. Moreover, the preparation process of microencapsulated PCM is quite complicated and the chemical reaction is difficult to control, so the cost of microencapsulated PCM is very high [20]. Considering these drawbacks, materials which have characteristics of porous, large specific surface area, and high conductivity have been used recently as matrix materials to prepare PCM [5,21–23]. Xu and Li [5] mixed diatomite powder and paraffin first and then put the mixture at temperature of (80 ± 5) °C for 4 h to produce diatomite powder/paraffin composite PCM. Through a series of experiments, it was found that the optimum paraffin percentage was 47.4% and the specific latent heat was 70.51 $J \cdot g^{-1}$.

Recycling construction and demolition wastes to partially replace Portland cement is a potential sustainable approach that can effectively reduce greenhouse gas emissions from the cement and concrete industries [24], thus alleviating the sustainability challenges faced by these industries. RBA is construction and demolition waste generated from retrofitting and demolition of existing structures. RBA is a porous material [25] which can be used as a good supporting matrix for PCM. Mankel et al. [13] prepared paraffin/recycled brick aggregate composite PCM by an advanced spray process. The paraffin/RBA composite PCM showed a good thermal energy storage property. Some studies also reported that paraffin/RBA composite PCM prepared by vacuum impregnation of fine aggregate from crushing concrete blocks have high thermal energy storage capacity [12]. However, crushing construction and demolition wastes into aggregates will generate a large amount of waste powder which is very difficult to utilize. Some researchers discovered that recycled brick powders (BP) with diameters less than 75 μm have pozzolanic activity and thus could partially replace cement in concrete [26]. In addition, BP has the characteristics of porosity, large specific surface area, and high conductivity. Utilizing BP as a type of support matric for PCM is an important green application of resources and has great environmental and economic benefits. However, few studies have focused on this topic.

In this study, BP which acts as a paraffin support matrix was used to prepare a shape-stabilized PCM. The characteristics of paraffin/BP composite PCM were tested. In general, there are multiple factors that determine whether the thermal energy storage cement-based materials are feasible in building applications, including encapsulation methods, phase change temperature, types of PCMs, architecture engineering, and regional weather. The surface of a building envelope structure can easily rise to 45 °C or more in the summer, and the temperature of the roof can reach nearly 70 °C [27,28]. According to previous studies, PCM with a high phase change temperature offered prospective application opportunities for improving building energy efficiency [5,29]. So, in this research, paraffin with a high phase change temperature was used. Besides the good thermal properties of PCM, its impact on the performances of materials based on cement is also important. PCM has considerable effects on the performances of cement-based materials in both early and later periods. Previous studies found when the cement replacement ratio was lower than 30%, mixed brick powder displayed a non-obvious or even favorable impact on the mechanical characters of concrete [30,31]. Hence, paraffin/BP composite were applied in this study to replace cement at replacement ratios of 10%, 20%, and 30%, according to the cement weight. Rheology properties, mechanical properties, volume stability, as well as thermal properties of thermal energy storage recycled mortar (TESRM) were examined.

2 Materials and methods

2.1 Materials

The ordinary portland cement (OPC) with a 28-d compressive strength of 42.5 MPa was used in this study, and the particle size distribution and chemical composition of OPC are shown in Fig. 1 and Table 1, respectively. Sand with a maximum size of 2.36 mm was also used in this study, and its sieve curve is shown in Fig. 1. The solid content of polycarboxylate superplasticizer (SP) was 20%.

The waste bricks were obtained from a construction demolition site. The waste bricks were placed into an impact crusher to obtain fine brick aggregates with a size smaller than 4.75 mm. After that, small pieces of crushed waste clay bricks were ground with a ball mill for 15 min to make BP. As demonstrated in Table 1, the chemical constitution of BP was observed via XRF, X-ray fluorescence spectrometer. The total amounts of SiO_2, Al_2O_3, and Fe_2O_3 were 68.31%, which satisfied the requirements of pozzolanic material of 50% according to ASTM C618, demonstrating that BP may have pozzolanic reactivity. The Morphologies of BP in both macro- and micro-scales are shown in Figs. 2(a) and 2(b). The distribution of particle size regarding BP was determined using a particle size analyzer (Winner 3000), and is shown in Fig. 2 (c). The porosity of BP was observed by mercury intrusion porosimetry (MIP, AutoPore Iv 9510), and is demonstrated in Fig. 2(d). The basic properties of BP are given in Table 2, such as average particle dimension (d_{50}), specific surface area, porosity, density and water requirement for standard consistency. The specific surface area was surveyed via the BET method (Brunauer–Emmett–Teller, ASAP2460). With a porosity of 0.0497 $mL \cdot g^{-1}$, BP showed a strong theoretical absorption capacity for paraffin. The density of the BP was measured according to the Chinese standard GB/T 208 and identified as 2.74 $g \cdot cm^{-3}$. To achieve standard consistency, the water demand of the

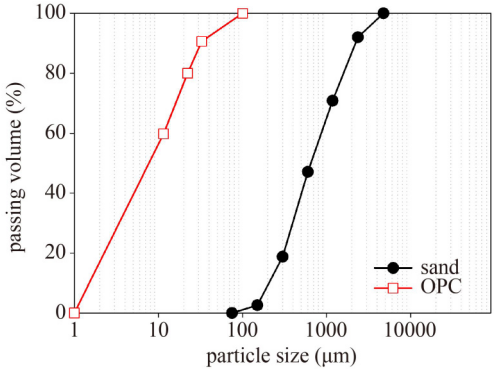

Fig. 1 Particle size distribution of river sand and OPC.

Table 1 Chemical compositions of OPC and BP (wt. %)

material	CaO	SiO_2	Al_2O_3	Fe_2O_3	SO_3	MgO	K_2O	Na_2O	TiO_2
OPC	58.01	23.19	9.21	3.66	2.62	1.36	1.02	0.40	0.41
BP	21.89	45.81	15.83	6.67	2.39	2.72	2.57	1.14	0.85

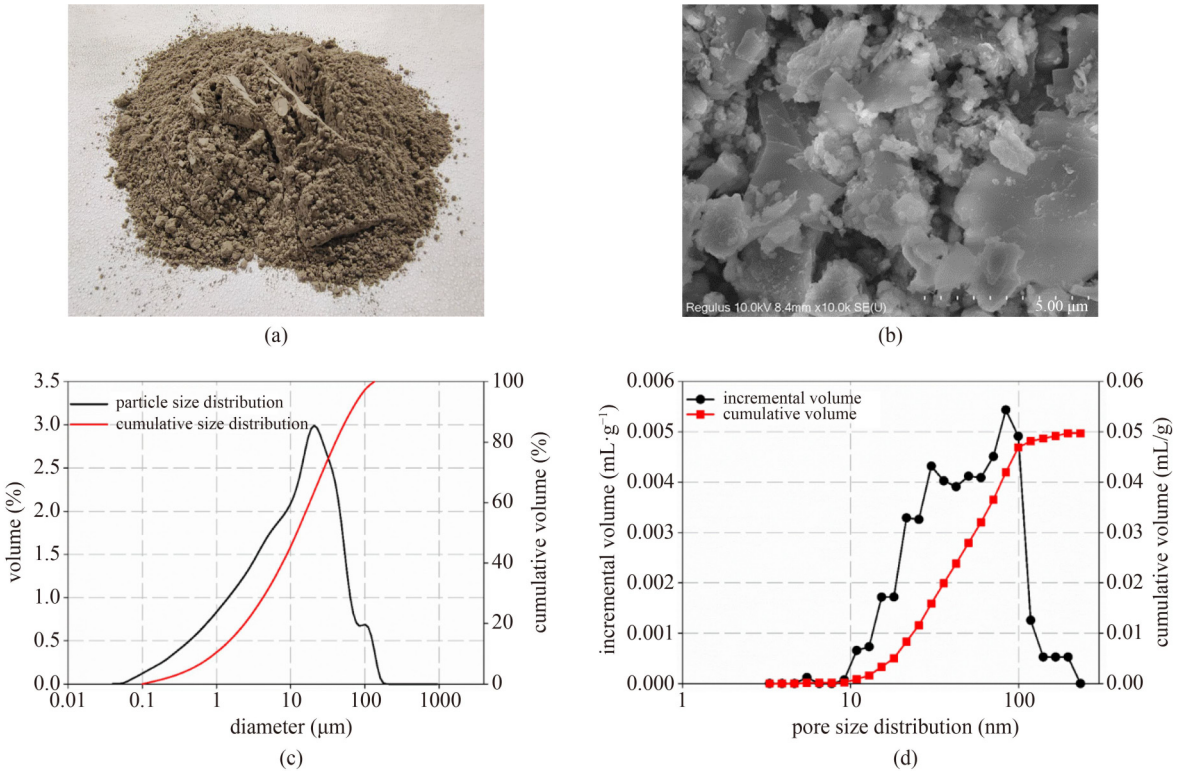

Fig. 2 The morphology, particle size distribution and pore size distribution of BP: (a) morphology; (b) micro-morphology; (c) particle size distribution; (d) pore size distribution.

Table 2 Basic properties of BP

d_{50} (μm)	S_{pore} ($m^2 \cdot g^{-1}$)	porosity ($mL \cdot g^{-1}$)	density ($g \cdot cm^{-3}$)	water requirement of standard consistency (%)
12.19	6.346	0.0497	2.74	30.1%

cement pastes with 20% BP was about 30.1%, which was measured according to BS EN 196e3:2005.

2.2 Paraffin/BP composite PCM preparation

Figure 3 demonstrates the schematic of the paraffin/BP composite PCM preparation process. Paraffin particles were first dry-mixed with BP at 700 r·min^{-1} for 2 min; thereafter, the paraffin/BP mixture was stored in a heating chamber at 100 °C for 2 h. To increase the pozzolanic activity of paraffin/BP composite PCM, the mixture was ball-milled for 5 min. Four mixtures were prepared with paraffin to BP weight ratios of 0.1:1, 0.2:1, 0.3:1, and 0.4:1. The corresponding theoretical weight percentages of paraffin were 9.1%, 16.7%, 23.1%, and 28.6%, respectively. It was found that after heating the paraffin/BP composite PCMs with 9.1%, 16.7%, and 23.1% paraffin were still in powder state, but the one with 28.6% paraffin was agglomerated into aggregates, indicating the overload of paraffin. As expected, the composite PCM with 23.1% paraffin had higher latent heat than those with 9.1% and 16.7%. Therefore, the ratio between paraffin and BP of 0.3:1, which the weight percentage of paraffin is 23.1%, was considered the best choice for preparing paraffin/BP composite PCM. Many researchers have implemented paraffin with a low phase change temperature 22–28 °C within the building indoor environment [6,13]. To regulate the temperature of building exterior walls and roofs, PCMs with higher phase change temperatures than those used in indoor environments should be chosen. This will reduce the temperature difference between the exterior and interior surfaces of the walls and roofs, thereby reducing heat conduction. With this consideration, paraffin with a phase change temperature of about 46.38 °C was used in this study. The thermo-physical characteristics of this paraffin are listed in Table 3. The latent heat, density, thermal conductivity and specific heat capacity of the paraffin were 145.10 J/g, 0.91 g·cm^{-3}, 0.15 W·m^{-1}·K^{-1} and 2.12 kJ·kg^{-1}·K^{-1}, respectively. The detailed characteristics of the paraffin are given in the latter part of this paper.

2.3 Characterization of paraffin/BP composite PCM

The micro morphology of paraffin/BP composite PCM was examined by scanning electron microscopy (SEM, model No. SU8100). The energy-dispersive X-ray spectroscopy (EDS) detector was used to test the elements of the paraffin/BP composite. The particle size distribution of the paraffin/BP composite was tested using a particle size analyzer (Winner 3000). FT-IR (Fourier transform infrared, Thermofisher IS50) spectroscopy was used to assess the chemical compatibility between paraffin and BP with the wavenumber ranging from 4000 to 400 cm^{-1}. The thermal properties of the paraffin/BP composite PCM were evaluated by DSC (Differential Scanning Calorimetry, TAQ600). For this, the temperature changed from 20 to 120 °C at a rate of 4 °C/min in a nitrogen atmosphere. The thermal stability of the paraffin/BP composite PCM was assessed in the temperature range of 20–400 °C at a heating rate of 10 °C/min by using the TGA (thermogravimetric analysis, TAQ600) method.

2.4 Mix and properties of TESRM

2.4.1 Mix designs

Paraffin/BP composite PCM was used to substitute cement at various ratios in order to study the effect on the rheology, mechanical, and thermal characteristics of cement mortar. It has been found in a previous study that replacing up to 30% of cement with recycled powder has the least negative effect on the mechanical properties [32]. Thus, in this study, the replacement ratio of paraffin/BP composite PCM was kept at no more than 30% and selected as 0%, 10%, 20%, and 30% by weight of cement. Mix proportions are listed in Table 4. The sand-to-binder ratio was 1.5, the water-to-binder (w/b) was 0.4 and an SP which could reduce the water demand of mortar by 25% was used in the mortar mix.

2.4.2 Rheology test

The rheological test was conducted by using a Brookfield rheometer as displayed in Fig. 4(a) according to the Chinese standard GB/T 2419 [33]. There was a 60 mm high and 30 mm diameter vane with four blades on the rheometer, as shown in Fig. 4(b). The mortar was filled in a 90 mm diameter and 500 mL volume container. To maintain the temperature at 20 °C, there was a temperature controlling device (Laudr E200) in contact with the container. In our research, the experiment was regulated

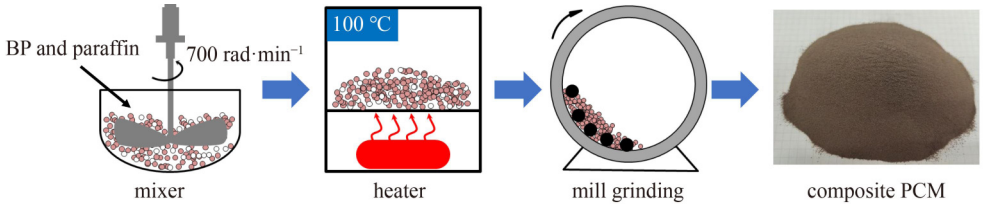

Fig. 3 Schematic of the composite PCM preparation.

primarily via shear rate, as displayed in Figs. 4(c) and 4(d). Two test procedures were used, one was for dynamic yield stress and plastic viscosity, and the other was for static yield stress. After mixing fresh mortar for about 2 min, the static yield stress and dynamic yield stress regarding fresh mortar were tested. The test procedure for dynamic yield stress is shown in Fig. 4(c). We pre-sheared the mortar at a velocity of 40 s^{-1} for 80 s and rested them for another 60 s in order to acquire a uniform status. Subsequently, the shear rate grew from 0 to 50 s^{-1} in the first 60 s and then dropped from 60 to 0 s^{-1} in the next 60 s. With a shear ratio of 10–50 s^{-1}, the descending curve was applied so as to compute the rheological parameters via the Bingham model [34]. The equation of the Bingham model, which was used to calculate the rheological parameters of conventional flowable concrete, is listed in Eq. (1).

$$\tau = \tau_0 + \mu\gamma, \tag{1}$$

where τ_0 is dynamic yield stress (Pa); μ is plastic viscosity (Pa·s); γ is shear rate (s^{-1}); τ is shear stress (Pa).

The test procedure of static yield stress is demonstrated in Fig. 4(d). The shear rate was maintaining a constant

Table 3 Thermo-physical characteristic of paraffin

property	value
melting temperature (°C)	46.38
total fusion latent heat (J/g)	145.1
density	0.91
specific heat ($kJ \cdot kg^{-1} \cdot K^{-1}$)	2.12
thermal conductivity ($W \cdot m^{-1} \cdot K^{-1}$)	0.15
major elements	C and H

Table 4 Mix proportions

sample	cement (g)	paraffin/BP composite PCM (g)	sand (g)	w/b[b)]	SP[c)] (%)
NM[a)]	1000	0	1500	0.4	0.5
TESRM10[a)]	900	100	1500	0.4	0.5
TESRM20	800	200	1500	0.4	0.5
TESRM30	700	300	1500	0.4	0.5

Notes: a) NM: normal mortar; TESRM: thermal energy storage recycled powder mortar; 10 = replacement ratio of paraffin/BP composite PCM is 10; b) w/b: water/binder ratio; c) SP: polycarboxylate superplasticizer.

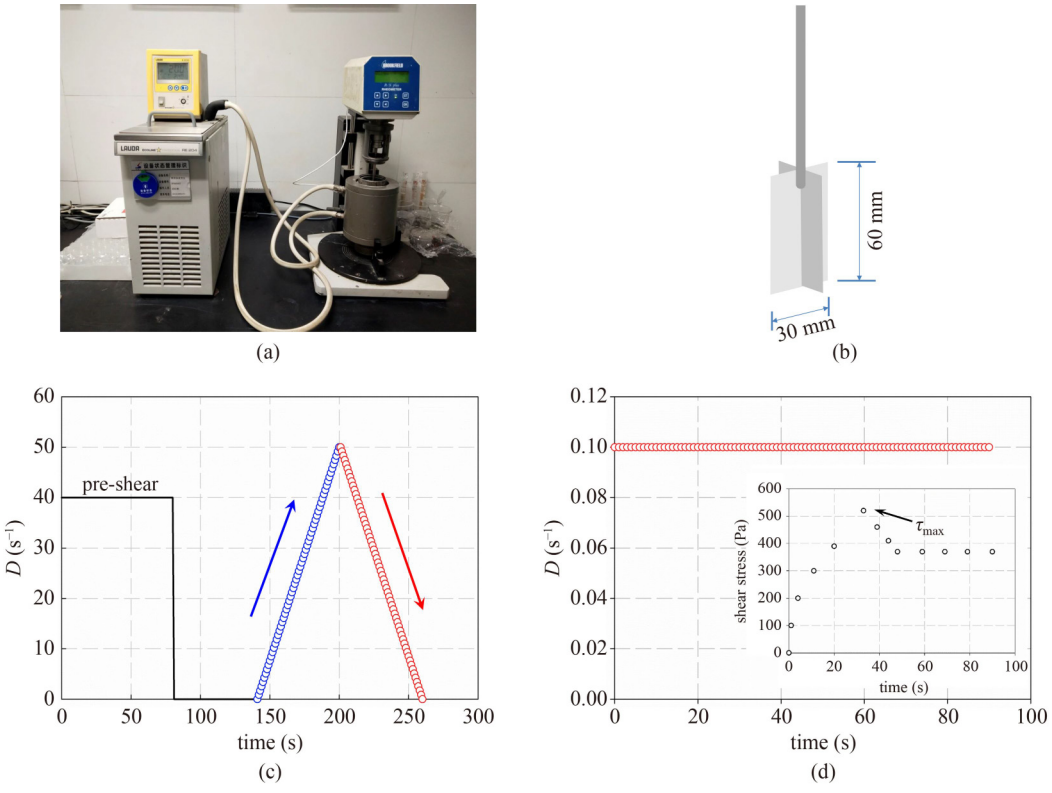

Fig. 4 Rheological test of TESRM: (a) Brookfield rheometer; (b) the four-bladed vane; (c) dynamic yield stress test procedure; (d) static yield stress test procedure.

value of 0.1 s^{-1} for 90 s. The peak value of shear stress curve was the static yield stress (τ_{max}).

2.4.3 Mechanical property test

According to the Chinese code JGJ/T70 [35], prisms with dimensions of 40 mm × 40 mm × 160 mm were prepared for determining their density, flexural strength and compressive strength. Prism samples were cast in steel molds, compacted via a vibrating table and taken out of the molds one day later. Samples were cured in a water tank with a temperature of (20 ± 2) °C before conducting the tests after 7, 28, and 90 d. For elastic modulus, the samples needed to be preloaded from 0.5 MPa to 1/3 of peak stress. After that, the samples were loaded to failure at a rate of 0.1 MPa·s^{-1}. In the range of elastic deformation, the elastic modulus can be obtained by using the relationship between stress and strain. Two strain gauges were pasted on the opposite sides of the prism in order to check deformation performance.

2.4.4 Volume stability test

Following ASTM C596-09 [36], specimens with dimensions of 25 mm × 25 mm × 285 mm were prepared for determining the volume stability of TESRM. After those specimens were cured in a standard curing room at (20 ± 0.5) °C and relative humidity 95% ± 2% for 2 d, the initial lengths were recorded. Then, specimens were cured within a room at (20 ± 0.5) °C and R.H. 50% ± 5%. Sample lengths were periodically measured until the curing age of 120 d.

2.4.5 Thermal performance test

Cubic specimens, 40 mm × 40 mm × 40 mm in size, were cast for the thermal conductivity test using the transient hot wire method [37]. Specimens were cured for 28 d at (20 ± 2) °C and R.H.95%. Before testing, samples were oven-dried at 105 °C for 24 h to remove free water. The overall thermal performance of NM and TESRM samples were compared by using a self-designed experimental setup as shown in Fig. 5. The two polyurethane boxes in this experiment were 400 mm × 400 mm × 400 mm in internal size and 50 mm wall thickness. One was a heating box equipped with a 100-W infrared lamp and a thermal meter that measured the temperature inside the heating box. The other box simulated the climate inside a building. A sample with dimensions of 200 mm × 200 mm × 30 mm was placed in the center of the box, and the temperature of the sample's central inner surface was measured with a thermal meter. Four heating-cooling cycles were used to evaluate the thermal performance of the NM and TESRM. The heating and cooling times were set to be approximately 50 and 180 min, respectively.

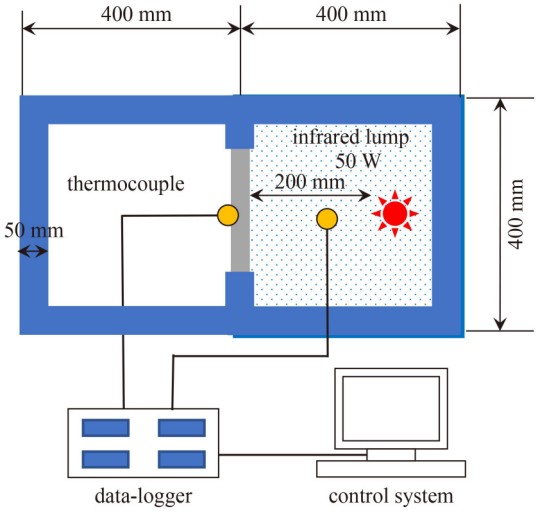

Fig. 5 Schematic of experimental setup for testing mortar thermal performance.

After the last cycle, the sample was allowed to cool naturally to room temperature.

3 Results and discussion

3.1 Characterization of paraffin/BP composite PCM

The appearance of the paraffin/BP composite PCM in micro and macro is shown in Figs. 6(a) and 6(b). The paraffin was incorporated into the BP, and there was some paraffin on the surface of the BP particles. The element content of the composite PCM particle was tested using the EDS. As indicated in Fig. 6(c), carbon, C, accounts for up to 56.36% of the content element by element. Hydrogen and carbon are the two primary components of paraffin.

Figure 7 shows the particle size distribution and cumulative size distribution of BP and paraffin/BP composite PCM. Although both BP and paraffin/BP composite PCM had large volume particles in the range of 10–100 μm, the mean diameter of paraffin/BP composite PCM was larger than that of BP. The mean diameters (d50) of BP and paraffin/BP composite PCM were 12.19 and 20.71 μm, respectively. This is mainly because some paraffin was covered on the BP surface, as shown in Fig. 6(b). Hence, the coarse particle volume tended to increase.

The FT-IR results of paraffin, BP, and paraffin/BP composite are displayed in Fig. 8. Further assignments of the characteristic bands are displayed in Table 5. The four distinctive absorption bands of paraffin were located at 719, 1473, 2849, and 2918 cm^{-1}. Methylene group rocking and C-H bending were represented by the bands at 719 and 1473 cm^{-1}, respectively, while C-H stretching was represented by the bands at 2849 and 2918 cm^{-1}. The

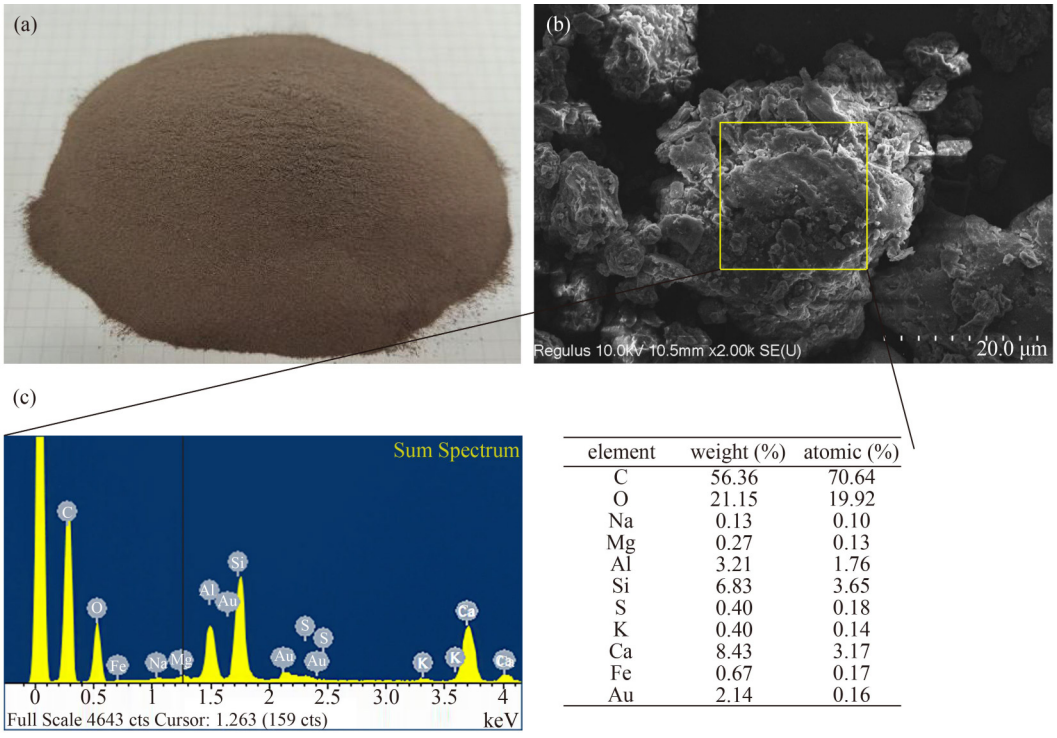

element	weight (%)	atomic (%)
C	56.36	70.64
O	21.15	19.92
Na	0.13	0.10
Mg	0.27	0.13
Al	3.21	1.76
Si	6.83	3.65
S	0.40	0.18
K	0.40	0.14
Ca	8.43	3.17
Fe	0.67	0.17
Au	2.14	0.16

Fig. 6 Appearance and microstructure of the paraffin/BP composite PCM: (a) appearance; (b) SEM morphology, (c) EDS result.

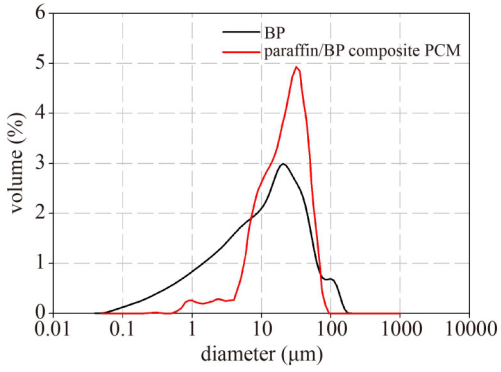

Fig. 7 Particle distribution of BP and paraffin/BP composite PCM.

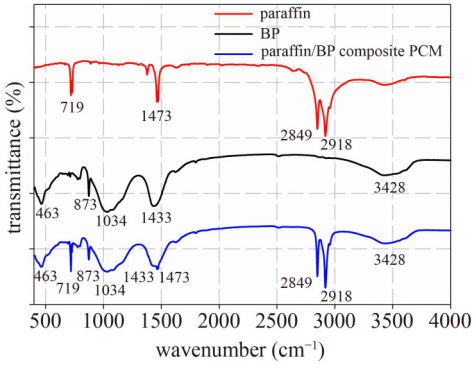

Fig. 8 FI-TR of BP, paraffin and paraffin/BP composite PCM.

BP bands were 463, 873, 1034, 1433, and 3428 cm^{-1}, which corresponded to the stretching of Si-O-Si, Al-Fe-OH, Si-O, O-C-O, and Al-O-H, respectively. The bands at 463, 873, 1034, 1433, and 3428 cm^{-1} in the paraffin/BP 30 composite PCM were connected to BP, whereas paraffin was linked to the bands at 719, 1473, 2850, and 2918 cm^{-1}. Comparing the FT-IR results of paraffin, BP, and paraffin/BP composite indicated that no new chemicals had developed and paraffin and BP were chemically compatible.

Figure 9 shows the DSC results of paraffin and paraffin/BP composite PCM. Table 5 provides a summary of the results for specific latent heat (H_M), peak melting temperature (T_{peak}), and onset melting temperature (T_{onset}). The T_{onset}, T_{peak}, and H_M of paraffin during the melting procedure were 46.38 °C, 84.91 °C, and 145.1 $J \cdot g^{-1}$, respectively. During the freezing procedure, T_{onset}, T_{peak} and H_M of paraffin were 96.72 °C, 81.14 °C, and 136.9 $J \cdot g^{-1}$, respectively. The T_{onset} and T_{peak} of paraffin/BP composite PCM during the melting and freezing processes were slightly shifted when compared to those of paraffin. The T_{onset} of paraffin/BP composite PCM in melting process was 46.49 °C and while in the freezing process was 91.6 °C. This might be because paraffin and BP physically interacted, and the elements in the composite influenced which way the melting point shifted [38]. During the melting and freezing processes, the latent heat of the paraffin/BP composite PCM was 30.10 and 28.44 $J \cdot g^{-1}$, respectively.

The H_M values of paraffin/BP composite PCM obtained from DSC curves are presented in Table 6. The theoretical specific latent heat value (H_T) of paraffin/BP composite PCM was determined using Eq. (2) [39].

Table 5 Assignments of the FTIR characteristic bands of paraffin, BP and paraffin/BP composite PCM

group	Si-O-Si	$-CH_2$	Al-Fe-OH	Si-O	O-C-O	$-CH_2$ and $-CH_3$	Al-O-H
BP	463	–	873	1034	1433	–	3428
paraffin	–	719	–	–	–	1473, 2849, 2918	–
paraffin/BP composite PCM	463	719	873	1034	1433	1473, 2849, 2918	3428

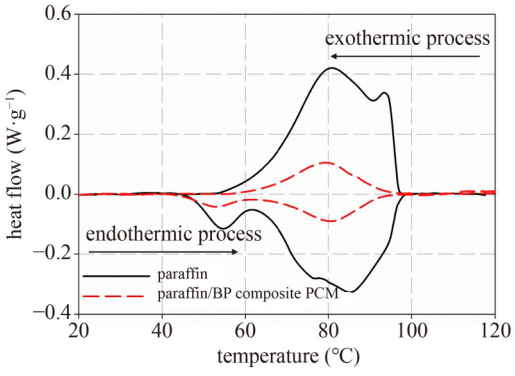

Fig. 9 Measured DSC curves of paraffin and paraffin/BP composite PCM.

$$H_T = H_{paraffin} \times W_{paraffin}, \quad (2)$$

where H_T represents theoretical latent heat value ($J \cdot g^{-1}$); $H_{paraffin}$ is latent heat value of paraffin ($J \cdot g^{-1}$); $W_{paraffin}$ represents weight ratio of paraffin to BP.

According to Eq. (1), the H_T values of paraffin/BP composite PCM were 33.52 and 31.59 $J \cdot g^{-1}$ during melting and freezing process, respectively, which were close to the H_M value, indicating that paraffin was well impregnated into BP materials.

TGA techniques were used to assess the thermal stability of the paraffin/BP composite. The thermal deterioration of paraffin/BP composite PCM and paraffin are shown in Fig. 10. The mass decrease in paraffin/BP composite PCM started around 155 °C and concluded around 300 °C. The paraffin weight reduction began around 145 °C and ended at about 245 °C. Therefore, it indicates that paraffin's heat stability increased as a result of being impregnated into BP. A later significant weight decrease of paraffin/BP composite PCM may have been due to the difference in physical activity between free paraffin and paraffin combined with pores. The paraffin/BP composite showed an overall weight decrease of 21.6%, which was close to the anticipated 23.1%. It demonstrated that the paraffin/BP composite mixture was prepared uniformly.

3.2 Rheological property of TESRM

The effect of the paraffin/BP composite PCM replacement ratio on the density and flow of TESRM is shown in Fig. 11. For replacement ratios of 10%, 20%, and 30%, the density decrease ratios were 6.37%, 7.14%, and 7.78%, respectively. The flow decreased obviously with the growth of the paraffin/BP composite PCM replacement ratio. Compared with NM, TESRM30 obtained a reduction of 28.8%. This may be attributed to two possible reasons. Firstly, BP was obtained from waste clay brick and some researchers reported that flow abilities of cement-based materials with BP could decline about 12% [40]. The other possible reason may be the absorption of superplasticizer by some paraffin covered on the surface of the composite PCM. Xu and Li [5] reported that when the composite PCM replacement level was increased from 0% to 30%, the SP dosage increased from 1.2% to 8% to maintain a flow at (165 ± 10) mm.

Figure 12 shows the rheological parameters of TESRM with different levels of paraffin/BP composite PCM. The dynamic yield stress and plastic viscosity could be calculated by the Bingham model. As displayed in Fig. 12, there was a strong liner relationship between shear rate and shear stress, and each determination coefficient (R^2) was above 0.98. The results of dynamic yield stress and plastic viscosity given in Table 7 showed that dynamic yield stress and plastic viscosity increased with the increasing proportions of paraffin/BP composite PCM. Although, the dynamic yield stress of TESRM30 was about 172.9% higher than NM, the dynamic yield stress of all TESRM samples was less than 100 Pa. The plastic viscosities of TESRM samples remained about 20%–30% higher than NM.

Figure 13 shows the shear stress evolutions regarding the fresh mixtures of NM and TESRM. Generally, the static shear stress of the sample first increased to a maximum and then decreased. In general, a large amount of flocculation structures are produced as cement contacts with water molecules, resisting the distortion within the shear procedure. Therefore, the shear stress increased

Table 6 Thermal parameters of paraffin and paraffin/BP composite PCM

group	melting process				freezing process			
	T_{onset} (°C)	T_{peak} (°C)	H_M ($J \cdot g^{-1}$)	H_T ($J \cdot g^{-1}$)	T_{onset} (°C)	T_{peak} (°C)	H_M ($J \cdot g^{-1}$)	H_T ($J \cdot g^{-1}$)
paraffin	46.38	84.91	145.10	–	96.72	81.14	136.9	–
paraffin/BP composite PCM	46.49	81.67	30.10	33.52	91.60	79.34	28.44	31.59

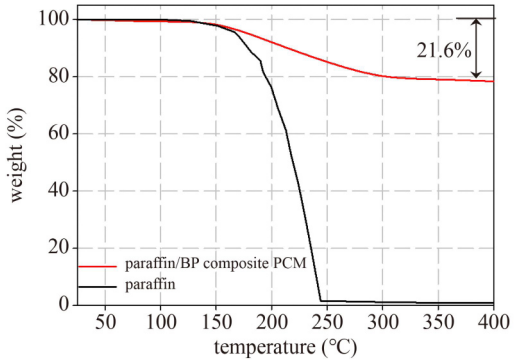

Fig. 10 TGA curves of paraffin and paraffin/BP composite PCM.

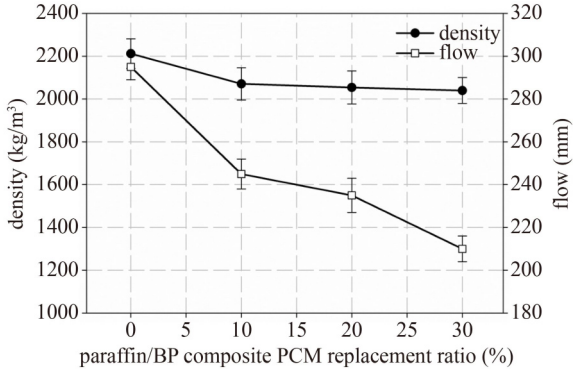

Fig. 11 Density and flow of TESRM with different paraffin/BP composite PCM replacement ratio.

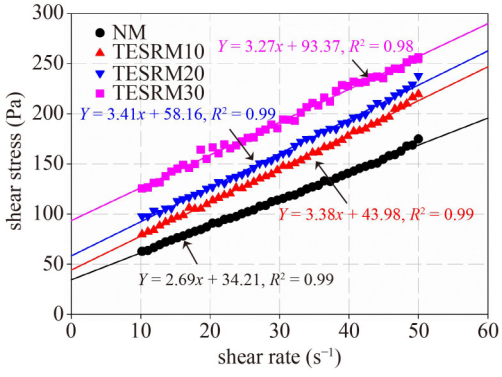

Fig. 12 Fitting curve of experimental results of NM and TESRM by Bingham model.

Table 7 Rheological properties of NM and TESRM samples

sample no.	dynamic yield stress (Pa)	plastic viscosity (Pa·s)	static yield stress (Pa)
NM	34.21 (0.0%)	2.69 (0.0%)	228.75 (0.0%)
TESRM10	43.98 (28.6%)	3.38 (25.7%)	632.65 (176.6%)
TESRM20	58.16 (70.0%)	3.41 (26.8%)	1038.99 (354.2%)
TESRM30	93.37 (172.9%)	3.27 (21.6%)	1354.60 (492.2%)

before the flocculation structure was broken. Afterwards, when the flocculation framework broke down, the fresh

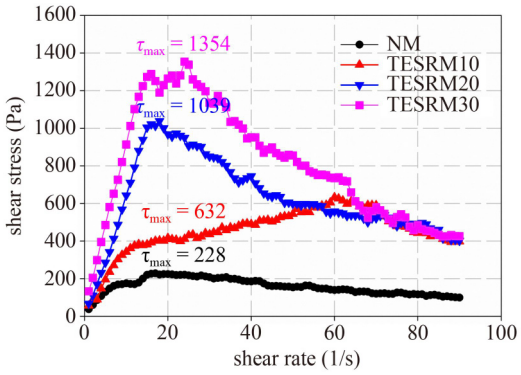

Fig. 13 Shear stress evolutions of the fresh mixtures of NM and TESRM.

mixture started to move and showed sticky liquid behavior [41], indicating a decrease in shear stress. The static yield stress increased significantly with the growth of the level of paraffin/BP composite PCM, as given in Table 7. The static yield stress of TESRM30 was 492.2% higher than that of NM, which could be attributed to the high water and superplasticizer absorption resulted from the presence of paraffin/BP composite PCM.

3.3 Mechanical properties of TESRM

Figure 14 demonstrates the compressive and flexural strengths of NM and TESRM specimens after 7, 28, and 90 d. As expected, strengths of all the TESRM samples were lower than the strength of the reference NM after all the investigated curing ages. As displayed in Fig. 14(a), the compressive strength regarding TESRM decreased with the increased of paraffin/BP composite PCM replacement ratio. Compared with the NM samples, the reductions of the compressive strength of TESRM10, TESRM20 and TESRM30 after 7 d were 26.25%, 37.97%, and 39.84%, respectively. However, the corresponding compressive strength reductions were 9.27%, 18.74%, and 24.6% after 90 d. This may have been due to the possible secondary hydration of BP in cement matrix at late ages. The compressive strength of recycled powder mortar decreased with the increased particle size of BP. The small particle size of BP improved the nucleation effect in cement-based materials, then improved the micro-structure of its newly made mortar. The mean diameter of paraffin/BP composite was 20.71 μm, which was far lower than 75 μm. Although the surface of BP was covered in part by paraffin, the addition of paraffin/BP composite also had a positive effect on the mechanical properties of mortar at later ages. Duan et al. [40] showed that the strength activity index of BP could be higher than 80%.

Figure 14(b) shows the flexural strength of TESRM samples after 7, 28, and 90 d. The trends of the flexural strength developments were similar to those of compressive strengths as displayed in Fig. 14(a). Compared with

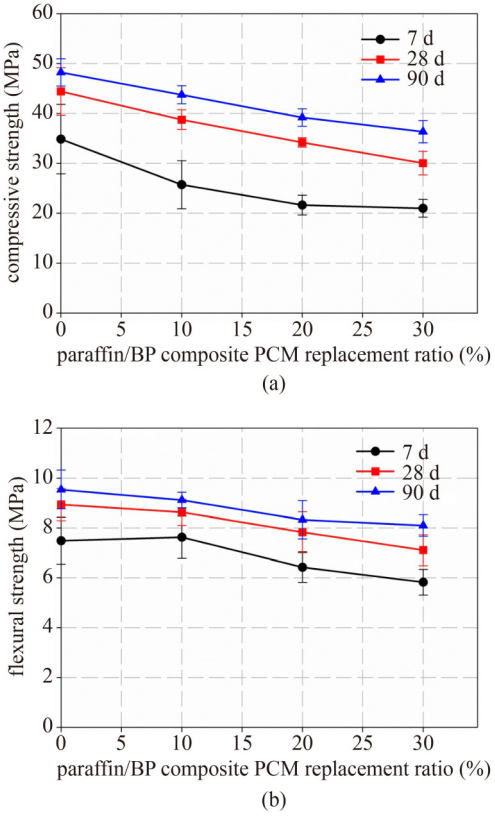

Fig. 14 Flexural and compressive strength of TESRM with different paraffin/BP composite PCM replacement ratio: (a) compressive strength; (b) flexural strength.

NM samples, the flexural strength reductions after 28 d were 3.44%, 12.4%, and 14.9% for TESRM10, TESRM20 and TESRM30 respectively. However, comparing the effects of paraffin/BP composite PCM on compressive strength and on flexural strength, it was found that the replacement percentage of the paraffin/BP composite had no significant effect on flexural strength. While the particle size of paraffin/BP composite powder was larger than that of BP powder due to paraffin covering the BP surface, some researchers found that the grain size does have an impact on the flexural strength of the mortar when the replacement ratio of BP powder is 10% [42,43]. This may explain why the flexural strength of TSERM10 is only slightly higher than that of NM. Although the strength of TESRM samples was lower than that of NM samples, its strength was still suitable for many applications that require moderate strength.

Figure 15 shows the elastic modulus of TESRM after 28 d. The trends of elastic modulus developments were similar to those of compressive and flexural strength. However, compared with NM the elastic modulus reduction of TESRM was much larger than compressive or flexural strength at the same paraffin/BP composite PCM replacement ratio. Compared with NM samples, the elastic modulus reductions of TESRM10, TESRM20 and TESRM30 were 18.29%, 34.17%, and 64.57%

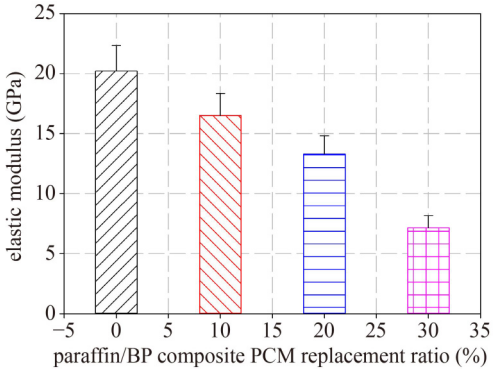

Fig. 15 Elastic modulus of TESRM with different paraffin/BP composite PCM replacement ratio.

respectively, after 28 d. From the SEM results of paraffin/BP composite PCM, some paraffin spilled out to cover part of the BP particle surfaces. As the paraffin/BP composite PCM particles were found evenly dispersed in the mortar matrix, there was lubrication between the particles. With the incorporation of paraffin/BP composite, the elastic modulus drastically decreased.

3.4 Drying shrinkage of TESRM

The length change results of TESRM and NM are shown in Fig. 16. As shown in Fig. 16(a), compared with NM, the addition of paraffin/BP composite PCM reduced the dry shrinkage. In addition, with the growth of the paraffin/BP composite PCM replacement ratio, dry shrinkage could be further reduced. After 120 d, the drying shrinkages of TESRM10, TESRM20 and TESRM30 at 28 d were 9.07%, 15.35%, and 26.15%, respectively. As reported in Refs. [44,45], pore microstructure of cement-based materials with BP could be refined at late age (≥ 90 d). In addition, paraffin is hydrophobic and can reduce water evaporation of cement-based materials [5]. These may be the reasons for the lower dry shrinkages of TESRM. As given in Fig. 16(b), drying shrinkage strain of TESRMs after 120 d showed a strong linear relationship with the replacement ratio of paraffin/BP composite PCM. The regressed correlation can be written as follows:

$$y = 13.77x - 1626.35,\ R^2 = 0.99, \tag{3}$$

where y is length change after 120 d (μm/m); x is level of paraffin/BP composite PCM (%).

3.5 Thermal properties of TESRM

The effect of paraffin/BP composite PCM replacement ratio on thermal conductivity of TESRM is shown in Fig. 17(a). The increase of the composite PCM level led to the decrease of the thermal conductivity of TESRM. When paraffin/BP composite PCM replacement levels

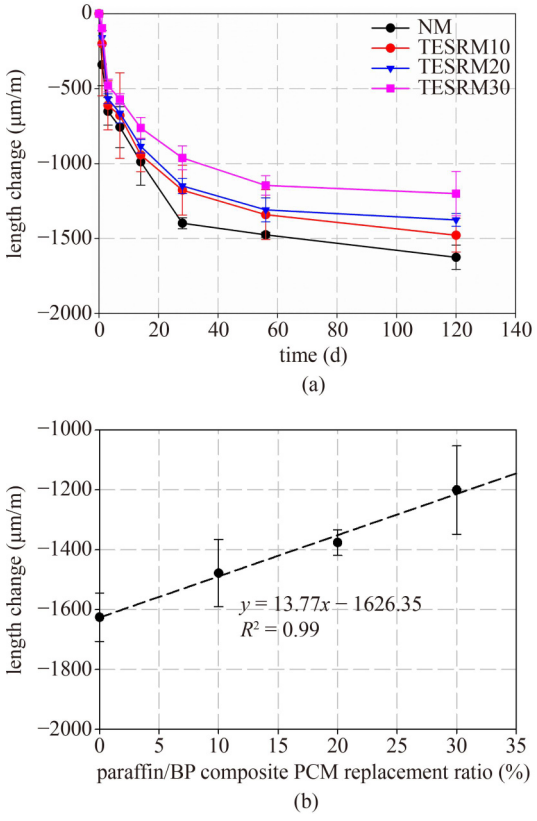

Fig. 16 Dry shrinkage of TESRM: (a) development of drying shrinkage; (b) regressed relationship between drying shrinkage after 120 d and the level of paraffin/BP composite PCM level.

were 10%, 20%, and 30%, the thermal conductivity reductions were 19.31%, 28.04%, and 36.33%, respectively, which may be because the thermal conductivity of paraffin (0.15 $W \cdot m^{-1} \cdot K^{-1}$) was much lower than that of cement and BP. A remarkable linear correlation can be obtained between paraffin/BP composite PCM dosages and thermal conductivity as follows:

$$y = -0.00203x + 1.667,\ R^2 = 0.95, \tag{4}$$

where y is the thermal conductivity of TESRM ($W \cdot m^{-1} \cdot K^{-1}$); x is paraffin/BP composite PCM replacement ratio (%).

Figure 17(b) shows the relationship between the thermal conductivity and density of TESRM. The increase of density led to an increase in thermal conductivity of TESRM. The density of mortar was an important factor affecting thermal conductivity. A linear relationship between thermal conductivity and density of TESRM could be obtained as follows:

$$y = 0.00322x - 5.388,\ R^2 = 0.91, \tag{5}$$

where y is the thermal conductivity of TESRM ($W \cdot m^{-1} \cdot K^{-1}$); x is density of TESRM ($kg \cdot m^{-3}$).

The thermal performance of NC and TESRM were compared as shown in Fig. 18. The profile of inner surface temperature is shown in Fig. 18(a). In each heating/cooling cycle, the lowest temperature of TESRM samples was about the same or even higher, despite the maximum inner surface temperature of TESRM being lower than that of the NM. As the composite PCM replacement ratio increased, the maximum inner surface

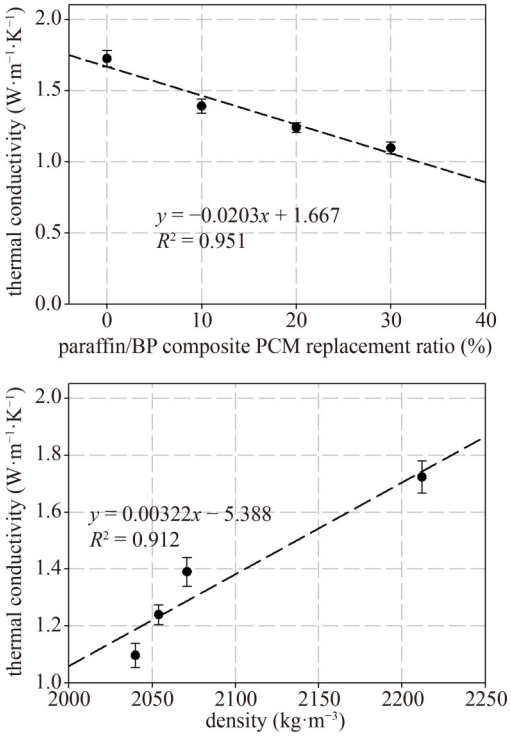

Fig. 17 Thermal conductivity of TESRM: (a) thermal conductivity of TESRM with different levels paraffin/BP composite PCM; (b) thermal conductivity of TESRM with different density.

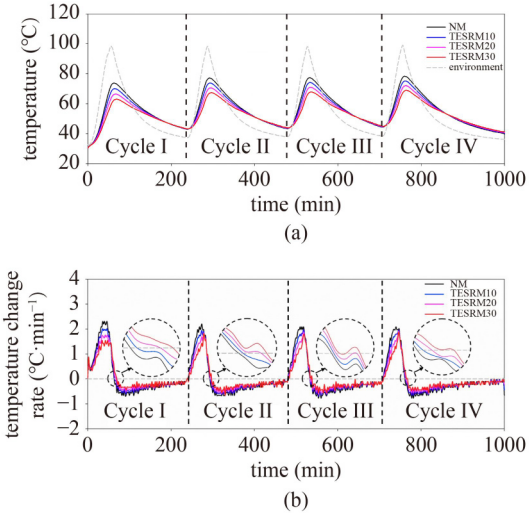

Fig. 18 Thermal performance comparison between NC and TESRM: (a) sample inner surface temperature comparison; (b) inner surface temperature change rate comparison.

temperature decreased. The maximum inner surface temperatures of NM, TESRM10, TESRM20, and TESRM30 were 77.2, 73.8, 70.5, and 67.1 °C, respectively. In addition, the temperature profile was almost the same in each heating/cooling cycle, which indicated that there was no paraffin leakage in the heating/cooling cycle.

Regardless of the heating or cooling operation, the temperature change rate of the TESRM sample was lower than that of the NC sample, as displayed in Fig. 18(b). Table 8 lists detail information on the NM and TESRM temperature change rates. The heating rate and the cooling rate of the TESRM30 sample were 29.6% and 33.7% respectively lower than those of the NM sample. In addition, all TESRM samples almost remained constant in each cycle regardless of the heating rate or cooling rate, which also proved that there was no paraffin leakage in heating/cooling cycles. In each heating/cooling cycle, the specimen took longer to transition from heating to cooling state, and this transition time increased with composite PCM content increased. The time for the TESRM30 sample to transition from the heating state to the cooling state was on average 7 min longer than that of the NM sample. Compared with the reduction of the temperature change rate, the phase delay was relatively short. The lower thermal conductivity and thermal energy storage characteristics of TSERM may both have caused the slow rate of temperature change. The incorporation of BP particles and paraffin both had a positive impact on thermal conductivity. The phase delay, however, was affected by the amount of phase change material and the latent heat value of phase change material. In this study, in order to maintain suitable mechanical properties, the amount of paraffin/BP composite PCM was 30% according to the cement weight so the paraffin was about 2.5% of total weight. Therefore, the phase delay was relatively short. In the future, the phase delay time can be further increased by increasing the amount of paraffin and latent heat value of paraffin.

According to the test results in this paper, paraffin/BP composite proved to be a promising candidate material for thermal storage in buildings. TERSM can be considered as a kind of structural-functional integrated material which can be used in traditional building applications. Besides good thermal properties, TESRM also maintains good mechanical properties. It can be used for building envelope structures to replace traditional plastering mortar, thus reducing building energy consumption. Moreover, some studies [46,47] reported that cementitious materials with appropriate dynamic yield stress and high static yield stress could be suitable for structural build-up of 3D printed cement materials. Therefore, it may indicate that cementitious materials with paraffin/BP composite PCM may be a suitable material for 3D printing.

4 Conclusions

A shape-stabilized phase change materials composite was developed in this study. TESRMs were also prepared by mixing this kind of phase change materials composite. Based on the above experimental results and intensive analysis, the following conclusions are put forward.

1) Paraffin/BP composite PCM was well prepared in this study and BP was successfully used as a support material for paraffin. The mean diameter of paraffin/BP composite PCM particles was larger than that of BP. Paraffin/BP composite PCM had good chemical compatibility and thermal stability. The prepared paraffin/BP composite had a melting temperature about 46.49 °C and the latent heat was 30.1 $J \cdot g^{-1}$. Therefore, the prepared paraffin/BP composite PCM is a promising candidate material for thermal storage in buildings.

2) The addition of paraffin/BP composite PCM decreased the flowability of TESRM. With increasing paraffin/BP composite PCM content, the plastic viscosity, dynamic and static yield stress increased significantly.

3) Paraffin/BP composite PCM had a positive effect on the mechanical properties of mortar at later ages, and could improve the dry shrinkage of mortar. The compressive and flexural strength of TESRM30 could reach about 75% and 85% of those of NM at 90 d and the maximum dry shrinkage reduction percentage was 26.15%.

4) Incorporation of paraffin/BP composite PCM significantly improved the thermal properties of TESRM. Compared with NM and TESRM 30, the thermal

Table 8 The temperature change rate of NM and TESRM

Cycle no.	heating rate ($°C \cdot min^{-1}$)				cooling rate ($°C \cdot min^{-1}$)			
	NM	TESRM10	TESRM20	TESRM30	NM	TESRM10	TESRM20	TESRM30
Cycle I	0.713	0.65	0.586	0.523	–0.167	–0.144	–0.121	–0.098
Cycle II	0.684	0.615	0.544	0.475	–0.182	–0.163	–0.144	–0.125
Cycle III	0.682	0.613	0.544	0.475	–0.188	–0.168	–0.149	–0.129
Cycle IV	0.682	0.612	0.541	0.471	–0.163	–0.147	–0.131	–0.114
mean	0.69	0.622	0.554	0.486	–0.175	–0.156	–0.136	–0.116

conductivity reduced from 1.723 to 1.097 $W \cdot m^{-1} \cdot K^{-1}$. Moreover, from the thermal performance setup, it can be concluded that the incorporation of paraffin/BP composite PCM can reduce energy consumption by decreasing the indoor temperature and heating/cooling rate. In summary, recycled powder mortar with paraffin/BP composite PCM can be considered as a kind of structural-functional integrated material, which not only has good thermal properties, but also maintains good mechanical properties.

Notations

TESRM: thermal energy storage recycled powder mortar
NM: normal mortar
BP: recycled brick powder
PCM: phase change materials
RBA: recycled brick aggregate
OPC: ordinary portland cement
SP: polycarboxylate superplasticizer
TGA: thermogravimetric analysis
EDS: energy-dispersive X-ray spectroscopy
SEM: scanning electron microscopy
MIP: mercury intrusion porosimetry
XRF: X-ray fluorescence spectrometer
DSC: differential scanning calorimetry
FT-IR: Fourier transform infrared
τ_{max}: Static yield stress
T_{onset}: onset melting temperature
T_{peak}: peak melting temperature
H_M: latent heat
H_T: theoretical latent heat value
$W_{paraffin}$: weight ratio of paraffin in composite phase change materials

Acknowledgements The financial support from the National Natural Science Foundation of China (Grant No. 52078358) is gratefully appreciated. National Key R&D Program of China (No. 2022YFE0198300) and the GCCRN Core Project 11 are highly acknowledged.

References

1. Asadi I, Shafigh P, Abu Hassan Z F B , Mahyuddin N B. Thermal conductivity of concrete—A review. Journal of Building Engineering, 2018, 20: 81−93
2. Singh Rathore P K , Shukla S K, Gupta N K. Potential of microencapsulated PCM for energy savings in buildings: A critical review. Sustainable Cities and Society, 2020, 53: 101884
3. Zhou D, Zhao C Y, Tian Y. Review on thermal energy storage with phase change materials (PCMs) in building applications. Applied Energy, 2012, 92: 593−605
4. Ramakrishnan S, Sanjayan J, Wang X, Alam M, Wilson J. A novel paraffin/expanded perlite composite phase change material for prevention of PCM leakage in cementitious composites. Applied Energy, 2015, 157: 85−94
5. Xu B, Li Z. Paraffin/diatomite composite phase change material incorporated cement-based composite for thermal energy storage. Applied Energy, 2013, 105: 229−237
6. Xu B, Ma H, Lu Z, Li Z. Paraffin/expanded vermiculite composite phase change material as aggregate for developing lightweight thermal energy storage cement-based composites. Applied Energy, 2015, 160: 358−367
7. Hunger M, Entrop A G, Mandilaras I, Brouwers H J H, Founti M. The behavior of self-compacting concrete containing micro-encapsulated phase change materials. Cement and Concrete Composites, 2009, 31(10): 731−743
8. Zhang Z, Fang X. Study on paraffin/expanded graphite composite phase change thermal energy storage material. Energy Conversion and Management, 2006, 47(3): 303−310
9. Lafdi K, Mesalhy O, Shaikh S. The effect of surface energy on the heat transfer enhancement of paraffin wax/carbon foam composites. Carbon, 2007, 45(11): 2188−2194
10. Li C, Wang M, Xie B, Ma H, Chen J. Enhanced properties of diatomite-based composite phase change materials for thermal energy storage. Renewable Energy, 2020, 147: 265−274
11. Kheradmand M, Castro-Gomes J, Azenha M, Silva P D, de Aguiar J L B, Zoorob S E. Assessing the feasibility of impregnating phase change materials in lightweight aggregate for development of thermal energy storage systems. Construction & Building Materials, 2015, 89: 48−59
12. Suttaphakdee P, Dulsang N, Lorwanishpaisarn N, Kasemsiri P, Posi P, Chindaprasirt P. Optimizing mix proportion and properties of lightweight concrete incorporated phase change material paraffin/recycled concrete block composite. Construction & Building Materials, 2016, 127: 475−483
13. Mankel C, Caggiano A, Koenders E. Thermal energy storage characterization of cementitious composites made with recycled brick aggregates containing PCM. Energy and Building, 2019, 202: 109395
14. Wang R, Ren M, Gao X, Qin L. Preparation and properties of fatty acids based thermal energy storage aggregate concrete. Construction & Building Materials, 2018, 165: 1−10
15. Navarro L, de Gracia A, Castell A, Álvarez S, Cabeza L. PCM incorporation in a concrete core slab as a thermal storage and supply system: Proof of concept. Energy and Building, 2015, 103: 70−82
16. Ren M, Wen X, Gao X, Liu Y. Thermal and mechanical properties of ultra-high performance concrete incorporated with microencapsulated phase change material. Construction and Building Materials, 2021, 273: 121714
17. Aguayo M, Das S, Maroli A, Kabay N, Mertens J C E, Rajan S D, Sant G, Chawla N, Neithalath N. The influence of microencapsulated phase change material (PCM) characteristics on the microstructure and strength of cementitious composites: Experiments and finite element simulations. Cement and Concrete Composites, 2016, 73: 29−41
18. Jayalath A, San Nicolas R, Sofi M, Shanks R, Ngo T, Aye L, Mendis P. Properties of cementitious mortar and concrete containing micro-encapsulated phase change materials. Construction and Building Materials, 2016, 120: 408−417

19. Pomianowski M, Heiselberg P, Jensen R L, Cheng R, Zhang Y. A new experimental method to determine specific heat capacity of inhomogeneous concrete material with incorporated microencapsulated-PCM. Cement and Concrete Research, 2014, 55: 22−34
20. Drissi S, Ling T C, Mo K H, Eddhahak A. A review of microencapsulated and composite phase change materials: Alteration of strength and thermal properties of cement-based materials. Renewable & Sustainable Energy Reviews, 2019, 110: 467−484
21. Biswas K, Lu J, Soroushian P, Shrestha S. Combined experimental and numerical evaluation of a prototype nano-PCM enhanced wallboard. Applied Energy, 2014, 131: 517−529
22. Wang X, Yu H, Li L, Zhao M. Experimental assessment on a kind of composite wall incorporated with shape-stabilized phase change materials (SSPCMs). Energy and Building, 2016, 128: 567−574
23. Liu Z, Zang C, Hu D, Zhang Y, Lv H, Liu C, She W. Thermal conductivity and mechanical properties of a shape-stabilized paraffin/recycled cement paste phase change energy storage composite incorporated into inorganic cementitious materials. Cement and Concrete Composites, 2019, 99: 165−174
24. Tang Y, Xiao J, Zhang H, Duan Z, Xia B. Mechanical properties and uniaxial compressive stress−strain behavior of fully recycled aggregate concrete. Construction and Building Materials, 2022, 323: 126546
25. Liu Q, Singh A, Xiao J, Li B, Tam V W. Workability and mechanical properties of mortar containing recycled sand from aerated concrete blocks and sintered clay bricks. Resources, Conservation and Recycling, 2020, 157: 104728
26. Xiao J, Ma Z, Sui T, Akbarnezhad A, Duan Z. Mechanical properties of concrete mixed with recycled powder produced from construction and demolition waste. Journal of Cleaner Production, 2018, 188: 720−731
27. Zhuang C, Gao Y, Zhao Y, Levinson R, Heiselberg P, Wang Z, Guo R. Potential benefits and optimization of cool-coated office buildings: A case study in Chongqing, China. Energy, 2021, 226: 120373
28. Shen H, Tan H, Tzempelikos A. The effect of reflective coatings on building surface temperatures, indoor environment and energy consumption—An experimental study. Energy and Building, 2011, 43(2−3): 573−580
29. Zhang Y, Liu J, Su Z, Lu M, Liu S, Jiang T. Preparation of low-temperature composite phase change materials (C-PCMs) from modified blast furnace slag (MBFS). Construction & Building Materials, 2020, 238: 117717
30. Ma Z, Li W, Wu H, Cao C. Chloride permeability of concrete mixed with activity recycled powder obtained from C&D waste. Construction & Building Materials, 2019, 199: 652−663
31. Ortega J M, Letelier V, Solas C, Moriconi G, Climent M Á, Sánchez I. Long-term effects of waste brick powder addition in the microstructure and service properties of mortars. Construction & Building Materials, 2018, 182: 691−702
32. Liu Q, Tong T, Liu S, Yang D, Yu Q. Investigation of using hybrid recycled powder from demolished concrete solids and clay bricks as a pozzolanic supplement for cement. Construction & Building Materials, 2014, 73: 754−763
33. GB/T 2419. Test Method for Fluidity of Cement Mortar. Beijing: Ministry of Housing and Urban-Rural Development of the People's Republic of China, 2005 (in Chinese)
34. Barnes H A, Hutton J F, Walters K. An Introduction to Rheology. Amsterdam: Elsevier Science, 1989
35. JGJ/70. Standard for Test Method of Performance on Building Mortar. Beijing: Ministry of Housing and Urban-rural Development, 2009 (in Chinese)
36. ASTM C596-09. Standard Test Method for Drying Shrinkage of Mortar Containing Hydraulic Cement. West Conshohocken, PA: ASTM, 2017
37. Rottmann M, Beikircher T, Ebert H. Thermal conductivity of evacuated expanded perlite measured with guarded-hot-plate and transient-hot-wire method at temperatures between 295 K and 1073 K. International Journal of Thermal Sciences, 2020, 152: 106338
38. Zhang D, Zhou J, Wu K, Li Z. Granular phase changing composites for thermal energy storage. Solar Energy, 2005, 78(3): 471−480
39. Xu B, Li Z. Paraffin/diatomite/multi-wall carbon nanotubes composite phase change material tailor-made for thermal energy storage cement-based composites. Energy, 2014, 72: 371−380
40. Duan Z, Hou S, Xiao J, Li B. Study on the essential properties of recycled powders from construction and demolition waste. Journal of Cleaner Production, 2020, 253: 119865
41. Norhasri M, Hamidah M S, Fadzil A M, Megawati O. Inclusion of nano metakaolin as additive in ultra high performance concrete (UHPC). Construction & Building Materials, 2016, 127: 167−175
42. Liu Q, Li B, Xiao J, Singh A. Singh. A, Utilization potential of aerated concrete block powder and clay brick powder from C&D waste. Construction & Building Materials, 2020, 238: 117721
43. Li Z, Ge Z, Yao Z, Gao Z. Mechanical properties of mortar with recycled clay-brick-powder. In: 11th International Conference of Chinese Transportation Professionals. Nanjing: American Society of Civil Engineers, 2011, 3379−3388
44. Y. Zhao, J. Gao, C. Liu, X. Chen, Z. Xu. The particle-size effect of waste clay brick powder on its pozzolanic activity and properties of blended cement. Journal of Cleaner Production, 2020, 242: 118521
45. Kong Z, Qiuyi L I, Zhang X, Guo Y, Wang Z. Eeffect of recycled powders on properties of dry-mixed masonry mortars. China Powder Science and Technology, 2016, 22(3): 46−52
46. Xia M, Nematollahi B, Sanjayan J. Printability, accuracy and strength of geopolymer made using powder-based 3D printing for construction applications. Automation in Construction, 2019, 101: 179−189
47. Buswell R A, Leal de Silva W R, Jones S Z, Dirrenberger J. 3D printing using concrete extrusion: A roadmap for research. Cement and Concrete Research, 2018, 112: 37−49